

# A composite likelihood approach to computer model calibration using high-dimensional spatial data

Won Chang, Murali Haran, Roman Olson, and Klaus Keller

June 8, 2021

## Abstract

Computer models are used to model complex processes in various disciplines. Often, a key source of uncertainty in the behavior of complex computer models is uncertainty due to unknown model input parameters. Statistical computer model calibration is the process of inferring model parameter values, along with associated uncertainties, from observations of the physical process and from model outputs at various parameter settings. Observations and model outputs are often in the form of high-dimensional spatial fields, especially in the environmental sciences. Sound statistical inference may be computationally challenging in such situations. Here we introduce a composite likelihood-based approach to perform computer model calibration with high-dimensional spatial data. While composite likelihood has been studied extensively in the context of spatial statistics, computer model calibration using composite likelihood poses several new challenges. We propose a computationally efficient approach for Bayesian computer model calibration using composite likelihood. We also develop a methodology based on asymptotic theory for adjusting the composite likelihood posterior distribution so that it accurately represents posterior uncertainties. We study the application of our new approach in the context of calibration for a climate model.

## 1 Introduction

Complex computer models are often used to approximate real-world processes. These models enable us to conduct virtual experiments that are useful for studying and un-

26 derstanding complex physical phenomena. A central source of uncertainty regarding  
27 computer models, and hence the behavior of the process they are approximating, stems  
28 from uncertainty about the value of model input parameters. It is, however, often possible  
29 to learn about model parameter values from observations of the system being modeled.  
30 Computer model calibration, the methods used to learn about these parameters, involves  
31 finding model parameter settings that produce computer model outputs that are most  
32 compatible with the observed realization of the process. Statistical computer model  
33 calibration is a formal approach to parameter inference based on observations and on  
34 computer model output at various parameter settings. A sound approach to computer  
35 model calibration accounts for various sources of uncertainties such as measurement er-  
36 ror and model structural errors, and results in a probability distribution that summarizes  
37 our knowledge about the parameters. Quantifying uncertainties about the parameters  
38 carefully is important as this allows for a rigorous quantification of uncertainties about  
39 projections based on the model. Here we consider computer model calibration for prob-  
40 lems where the observations and the model output are in the form of spatial data.

41 Computer model calibration can pose nontrivial inferential challenges. In many ap-  
42 plications computer model runs are computationally expensive. In this case, model runs  
43 are often available at only a limited number of parameter settings. A popular method to  
44 overcome this hurdle is the Gaussian process approach (cf. Sacks et al., 1989; Kennedy  
45 and O’Hagan, 2001). This method enables calibration with a limited number of model  
46 runs using probabilistic interpolation between the model runs. However, this approach  
47 faces computational challenges when applied to computer model output that are in the  
48 form of high-dimensional spatial data, which are increasingly common in modern science  
49 and engineering applications (see e.g. Higdon et al., 2009; Bhat et al., 2010, 2012; Chang  
50 et al., 2013).

51 Some approaches have been developed recently to resolve these computational issues  
52 (e.g. Bayarri et al., 2007; Higdon et al., 2008; Bhat et al., 2012; Chang et al., 2013). In this  
53 manuscript we propose a new Bayesian approach for calibration with high-dimensional  
54 spatial data using composite likelihood methods.

55 The basic idea of composite likelihood (Besag, 1975, 1977; Lindsay, 1988) is to ap-  
56 proximate the original likelihood as a product of computationally cheaper likelihoods.  
57 This approach can be easily adapted for spatial modeling in various ways such as con-  
58 ditional likelihood (Vecchia, 1988; Stein et al., 2004), pairwise likelihood (Heagerty and  
59 Lele, 1998; Curriero and Lele, 1999; Cooley et al., 2011), and block likelihood (Caragea  
60 and Smith, 2006; Eidsvik et al., 2013). Here we construct a calibration method based  
61 on block composite likelihood. In particular, we adopt the idea of hybrid composite  
62 likelihood proposed by Caragea and Smith (2006) that relies on two components: (i)  
63 dependence between block means and (ii) dependence within each block conditioning on  
64 its block mean. This composite likelihood approach allows for a substantial reduction  
65 in the computational burden for maximum likelihood inference with high-dimensional  
66 spatial data. Also, this opens up possibilities for flexible spatial covariance structure that  
67 vary depending on each block. Moreover, since the composite likelihood from the block  
68 composite likelihood framework is a valid probability model, no further justification is  
69 necessary for its use in Bayesian inference.

70 The remainder of this paper is organized as follows. In Section 2 we outline the basic  
71 model calibration framework using Gaussian random fields. In Section 3 we formulate the  
72 Bayesian calibration model using block composite likelihood, discuss relevant asymptotic  
73 theory and explain how Godambe information may be used to adjust posterior uncertainty  
74 when using composite likelihood. In Section 4 we describe an application of our method  
75 to a climate model calibration problem using 2-dimensional spatial patterns of ocean  
76 temperature change and a relevant simulated example. Finally, in Section 5, we conclude  
77 with a discussion and future directions for research.

## 78 **2 Calibration using Gaussian Processes**

79 Here we introduce our computer model calibration framework which consists of two stages:  
80 model emulation and parameter calibration (Bayarri et al., 2007; Bhat et al., 2012; Chang  
81 et al., 2013). We first construct an ‘emulator’, which is a statistical model interpolating

82 the computer model outputs as well as providing interpolation uncertainties (Sacks et al.,  
83 1989). Using the emulator, we find the posterior density of computer model parameters  
84 while taking into account important sources of uncertainty including interpolation uncer-  
85 tainty, model-observation discrepancy, and observational error (Kennedy and O’Hagan,  
86 2001).

We will use the following notation henceforth.  $Y(\mathbf{s}, \boldsymbol{\theta})$  is the computer model output at the spatial location  $\mathbf{s} \in \mathcal{S}$  and the parameter setting  $\boldsymbol{\theta} \in \Theta$ .  $\mathcal{S}$  is the spatial field that we are interested in, usually a subset of  $\mathbb{R}^2$  or  $\mathbb{R}^3$ .  $\Theta \subset \mathbb{R}^q$  is the open set of all possible computer model parameter settings with an integer  $q \geq 1$ . Let  $\{\boldsymbol{\theta}_1, \dots, \boldsymbol{\theta}_p\} \subset \Theta$  be a collection of  $p$  design points in the parameter space and  $\{\mathbf{s}_1, \dots, \mathbf{s}_n\} \subset \mathcal{S}$  be the set of  $n$  model grid locations.  $\mathbf{Y}_i = (Y(\mathbf{s}_1, \boldsymbol{\theta}_i), \dots, Y(\mathbf{s}_n, \boldsymbol{\theta}_i))^T$  is computer model output at the model grid locations at the parameter setting  $\boldsymbol{\theta}_i$ . The concatenated  $np \times 1$  vector of all computer model outputs is  $\mathbf{Y} = (\mathbf{Y}_1^T, \dots, \mathbf{Y}_p^T)^T$ . Note that typically  $p \ll n$  since computer model runs with high-resolution are computationally expensive. Finally, we let  $Z(\mathbf{s})$  be an observation at spatial location  $\mathbf{s}$  and  $\mathbf{Z} = (Z(\mathbf{s}_1), \dots, Z(\mathbf{s}_n))^T$  be the observational data, a spatial process observed at  $n$  locations.

**Model Emulation Using Gaussian Processes.** Following Bhat et al. (2012) and Chang et al. (2013), we construct a Gaussian process that interpolates computer model outputs as follows

$$\mathbf{Y} \sim N(\mathbf{X}\boldsymbol{\beta}, \Sigma(\boldsymbol{\xi}_y)),$$

87 where  $\mathbf{X}$  is an  $np \times b$  covariate matrix containing all the spatial locations and climate  
88 parameters (that is,  $\mathbf{s}_1, \dots, \mathbf{s}_n$  and  $\boldsymbol{\theta}_1, \dots, \boldsymbol{\theta}_p$ ) used to define the covariance matrix  $\Sigma(\boldsymbol{\xi}_y)$ .  
89  $\boldsymbol{\beta}$  and  $\boldsymbol{\xi}_y$  are the vectors of regression coefficients and covariance parameters respectively.  
90 We construct an interpolation process by finding the maximum likelihood estimate (MLE)  
91 of these parameters. This interpolation model provides the predictive distribution of a  
92 computer model run at any given location  $\mathbf{s} \in \mathcal{S}$  and  $\boldsymbol{\theta} \in \Theta$  (Sacks et al., 1989). We call  
93 this predictive process an emulator and denote it by  $\eta(\mathbf{s}, \boldsymbol{\theta})$ . Note that, throughout this  
94 paper,  $\boldsymbol{\beta}$  is set to be  $\mathbf{0}$  since the Gaussian process provides enough flexibility in modeling  
95 the output process.

96 **Model Calibration Using Gaussian Random Processes.** We model the observa-  
 97 tional data  $\mathbf{Z}$  by the following model,

$$\mathbf{Z} = \boldsymbol{\eta}(\boldsymbol{\theta}^*) + \boldsymbol{\delta}, \quad (1)$$

98 where  $\boldsymbol{\theta}^*$  is the true or fitted value of computer model parameter for the observational  
 99 data (Bayarri et al., 2007),  $\boldsymbol{\eta}(\boldsymbol{\theta}^*) = (\eta(\mathbf{s}_1, \boldsymbol{\theta}^*), \dots, \eta(\mathbf{s}_n, \boldsymbol{\theta}^*))^T$  is the emulator output at  
 100  $\boldsymbol{\theta}^*$  on the model grid, and  $\boldsymbol{\delta} = (\delta(\mathbf{s}_1), \dots, \delta(\mathbf{s}_n))^T$  is a term that includes both data-  
 101 model discrepancy as well as observational error. The discrepancy process  $\delta(\mathbf{s})$  is also  
 102 modeled as a Gaussian process with spatial covariance between the locations  $\mathbf{s}_1, \dots, \mathbf{s}_n$ .  
 103 Model calibration with high-dimensional spatial data leads to computational challenges  
 104 as described in the following section.

## 105 **3 Calibration with High-Dimensional Spatial Data**

106 In this section we briefly examine the challenges in model calibration using high-dimensional  
 107 spatial data and the existing approaches to the problem. We then proceed to the formu-  
 108 lation of our composite likelihood approach.

### 109 **3.1 Challenges with High-Dimensional Spatial Data**

110 The basic challenge with the approach in Section 2 stems from the fact that the com-  
 111 putational cost for a single likelihood evaluation is  $\mathcal{O}(n^3p^3)$ . For large  $n$ , evaluating  
 112 the likelihood function repeatedly when using algorithms like Markov chain Monte Carlo  
 113 (MCMC) can become computationally prohibitive. One can reduce the computational  
 114 cost by assuming a separable covariance structure between the spatial dependence and  
 115 the dependence due to computer model parameters, but the computational cost is still  
 116  $\mathcal{O}(n^3)$ , and hence does not scale well with  $n$ . The current approaches to overcome such  
 117 limitation for high-dimensional data rely on dimension reduction or basis expansion.  
 118 The dimension reduction approaches (Bayarri et al., 2007; Chang et al., 2013) map the  
 119 original output into a lower dimension and exploit the uncorrelated nature of the low-

120 dimensional processes to speed up the computation. The basis expansion approaches  
121 (Bhat et al., 2012; Higdon et al., 2008) use a basis representation of model output that  
122 results in a reformulated likelihood with a lower computational cost. Here we introduce  
123 a somewhat different approach that relies on the block composite likelihood for spatial  
124 data (Caragea and Smith, 2006; Eidsvik et al., 2013).

## 125 **3.2 Composite Likelihood for Model Calibration**

126 In this framework, we partition the spatial field  $\mathcal{S}$  into small blocks to avoid the com-  
127 putational issues related to high-dimensional data. In Section 4 we describe an example  
128 of how such a partition may be constructed in practice. The block composite likelihood  
129 method substitutes the original likelihood by a composite likelihood that utilizes the  
130 spatial blocks, thereby resulting in a likelihood function that requires much less com-  
131 putational effort. In particular, we adopt the block composite likelihood formulation  
132 by Caragea and Smith (2006). This framework assumes conditional independence be-  
133 tween outcomes in different blocks given the block means, and the dependence between  
134 blocks is modeled through the covariance between block means. Note that this framework  
135 gives a valid probability model, and therefore the posterior distribution defined using the  
136 composite likelihood function based on this approach is also a valid probability model.  
137 Obtaining a valid probability model is important because we are embedding the likeli-  
138 hood within a Bayesian approach; having a valid probability model automatically assures  
139 us that the resulting posterior distribution is proper when all the prior distributions used  
140 are proper.

We divide the spatial area for the computer model output into  $M$  different blocks and denote the output for each block by  $\mathbf{Y}_{(1)}, \dots, \mathbf{Y}_{(M)}$ . Note that the blocks are made according to the spatial field, not the parameter space, because the number of computer model runs is usually quite limited due to the high computational costs of running the model. However, in principle our approach may be extended to blocking in parameter space as well if the number of model runs is also large. Let  $n_i$  denote the number of computer model outcomes in the  $i$ th block. We denote the spatial locations in the  $i$ th

block by  $\mathbf{s}_{i1}, \dots, \mathbf{s}_{in_i}$ . Each  $\mathbf{Y}_{(i)}$  is a stack of  $(n_i - 1)$ -dimensional spatial output for  $p$  different parameter settings;

$$\mathbf{Y}_{(i)} = (Y(\mathbf{s}_{i1}, \cdot)^T, Y(\mathbf{s}_{i2}, \cdot)^T, \dots, Y(\mathbf{s}_{in_i-1}, \cdot)^T)^T,$$

141 where  $Y(\mathbf{s}_{ij}, \cdot) = (Y(\mathbf{s}_{ij}, \boldsymbol{\theta}_1), \dots, Y(\mathbf{s}_{ij}, \boldsymbol{\theta}_p))^T$  is the  $p \times 1$  vector of computer model out-  
 142 comes for all the parameter settings  $\boldsymbol{\theta}_1, \dots, \boldsymbol{\theta}_p$ . Note that we omit one spatial loca-  
 143 tion for each block in defining the output vectors to avoid degeneracy. We let  $\bar{\mathbf{Y}}_{(i)} =$   
 144  $\frac{1}{n_i} \sum_{j=1}^{n_i} (Y(\mathbf{s}_{ij}, \boldsymbol{\theta}_1), \dots, Y(\mathbf{s}_{ij}, \boldsymbol{\theta}_p))^T$  be the  $p$ -dimensional mean vector of model outcomes  
 145 for the  $i$ th block. That is, means for the spatial block consisting of same set of loca-  
 146 tions across all model parameter settings. We define the vector of all block means by  
 147  $\bar{\mathbf{Y}} = (\bar{\mathbf{Y}}_{(1)}^T, \dots, \bar{\mathbf{Y}}_{(M)}^T)^T$ . Similarly, we divide the observational data into  $M$  blocks in  
 148 the same way and omit one observation for each block to have  $\mathbf{Z}_{(1)}, \dots, \mathbf{Z}_{(M)}$ , the vectors  
 149 of observational data in different blocks. We let  $\bar{\mathbf{Z}}_{(i)} = \frac{1}{n_i} \sum_{j=1}^{n_i} Z(\mathbf{s}_{ij})$  be the  $i$ th block  
 150 mean of observational data and  $\bar{\mathbf{Z}} = (\bar{\mathbf{Z}}_{(1)}, \dots, \bar{\mathbf{Z}}_{(M)})^T$  be the collection of them.

Assuming separability, we model the covariance between the process at two different spatial locations and parameter settings  $Y(\mathbf{s}, \boldsymbol{\theta})$  and  $Y(\mathbf{s}', \boldsymbol{\theta}')$  by

$$\text{Cov}(Y(\mathbf{s}, \boldsymbol{\theta}), Y(\mathbf{s}', \boldsymbol{\theta}')) = K_s(\mathbf{s}, \mathbf{s}'; \boldsymbol{\xi}_s) K_\theta(\boldsymbol{\theta}, \boldsymbol{\theta}'; \boldsymbol{\xi}_\theta),$$

where  $K_s$  and  $K_\theta$  are valid covariance functions respectively in  $\mathcal{S}$  and  $\Theta$  with parameters  $\boldsymbol{\xi}_s$  and  $\boldsymbol{\xi}_\theta$ . The covariance between discrepancy process  $\mathbf{s}$  and  $\mathbf{s}'$  is given by

$$\text{Cov}(\delta(\mathbf{s}), \delta(\mathbf{s}')) = K_d(\mathbf{s}, \mathbf{s}'; \boldsymbol{\xi}_d)$$

151 with a valid covariance function  $K_d$  in  $\mathcal{S}$  and a vector of parameters  $\boldsymbol{\xi}_d$ . More specific  
 152 definition of the covariance functions will be discussed below.

**Computer Model Emulation.** The first component of our composite likelihood is the model for block means, which captures the large scale trend. The covariance between

the block means is

$$\Sigma^{\bar{\mathbf{Y}}} = \mathbf{H} \otimes \Sigma_\theta,$$

153 where  $\Sigma_\theta$  is the covariance matrix for the random variable across  $p$  parameter settings  
 154 and  $\mathbf{H}$  is the  $M \times M$  covariance matrix between the blocks. It is straightforward to see  
 155 that the block covariance is

$$\{\mathbf{H}\}_{ij} = \frac{1}{n_i n_j} \sum_{k=1}^{n_i} \sum_{l=1}^{n_j} K_s(\mathbf{s}_{ik}, \mathbf{s}_{jl}; \boldsymbol{\xi}_s), \quad (2)$$

156 the mean of all possible cross covariances between two blocks.

157 The second component is the sum of the conditional likelihoods for each block, which  
 158 models the small scale dependence and variation. For the  $i$ th block, the conditional  
 159 distribution of output  $\mathbf{Y}_{(i)}$  given the block mean  $\bar{\mathbf{Y}}_{(i)}$  is a normal distribution with the  
 160 mean and covariance given by

$$\begin{aligned} \mu_i^{\mathbf{Y}|\bar{\mathbf{Y}}} &= E(\mathbf{Y}_{(i)}|\bar{\mathbf{Y}}_{(i)}) = (\gamma^{(i)} / \{\mathbf{H}\}_{ii} \otimes I_p) \bar{\mathbf{Y}}_{(i)} \\ \Sigma_i^{\mathbf{Y}|\bar{\mathbf{Y}}} &= Var(\mathbf{Y}_{(i)}|\bar{\mathbf{Y}}_{(i)}) = (\Gamma_i - \gamma^{(i)} (\gamma^{(i)})^T / \{\mathbf{H}\}_{ii}) \otimes \Sigma_\theta \end{aligned}$$

161 where

$$\begin{aligned} \{\gamma^{(i)}\}_j &= \sum_{k=1}^{n_i} K_s(\mathbf{s}_{ij}, \mathbf{s}_{ik}; \boldsymbol{\xi}_s) / n_i, \quad j = 1, \dots, n_i - 1, \\ \{\Gamma_i\}_{jk} &= K_s(\mathbf{s}_{ij}, \mathbf{s}_{ik}; \boldsymbol{\xi}_s), \quad j = 1, \dots, n_i - 1, \quad k = 1, \dots, n_i - 1. \end{aligned}$$

162 Here,  $\Gamma_i$  is the spatial covariance matrix for the  $i$ th block and  $\gamma^{(i)}$  is the  $(n_i - 1) \times 1$   
 163 covariance vector between the  $i$ th block mean and the  $i$ th block locations. The log  
 164 composite likelihood function for the model output is then

$$\begin{aligned} cl(\boldsymbol{\xi}_s, \boldsymbol{\xi}_\theta) \propto & - \frac{1}{2} \left( \log |\Sigma^{\bar{\mathbf{Y}}}| + \bar{\mathbf{Y}}^T (\Sigma^{\bar{\mathbf{Y}}})^{-1} \bar{\mathbf{Y}} \right) \\ & - \frac{1}{2} \sum_{i=1}^M \left( \log |\Sigma_i^{\mathbf{Y}|\bar{\mathbf{Y}}}| + (\mathbf{Y}_{(i)} - \mu_i^{\mathbf{Y}|\bar{\mathbf{Y}}})^T (\Sigma_i^{\mathbf{Y}|\bar{\mathbf{Y}}})^{-1} (\mathbf{Y}_{(i)} - \mu_i^{\mathbf{Y}|\bar{\mathbf{Y}}}) \right), \end{aligned}$$



165 We construct the emulator by finding the MLE of  $\boldsymbol{\xi}_\theta$  and  $\boldsymbol{\xi}_s$ , denoted by  $\hat{\boldsymbol{\xi}}_\theta$  and  $\hat{\boldsymbol{\xi}}_s$ .  
 166 The computational cost for a single likelihood evaluation is reduced from  $\frac{1}{3}n^3$  flops to  
 167  $\sum_{i=1}^M \sum_{j=i}^M n_i n_j + \frac{1}{3}(M^3) + \frac{1}{3} \left( \sum_{i=1}^M (n_i - 1)^3 \right)$  flops, where the first term is the computa-  
 168 tional cost for finding H. This is a reduction from  $6.86 \times 10^{10}$  flops to  $5.92 \times 10^7$  flops in  
 169 the climate model calibration example in Section 4.

170 **Computer Model Calibration.** We formulate the composite likelihood for observa-  
 171 tional data in the same manner as above. Let  $\Omega$  be the  $M \times M$  covariance between the  
 172  $M$  block means of the discrepancy  $\boldsymbol{\delta}$ , defined in the same way as H with a different set of  
 173 parameters  $\boldsymbol{\xi}_d$ . The conditional mean and covariance for the block means of observational  
 174 data  $\bar{\mathbf{Z}}$  are

$$\begin{aligned} \mu^{\bar{\mathbf{Z}}} &= (I_M \otimes \Sigma_{\theta^* \theta} \Sigma_\theta^{-1}) \bar{\mathbf{Y}}, \text{ an } M \times 1 \text{ vector,} \\ \Sigma^{\bar{\mathbf{Z}}} &= H \otimes (\Sigma_{\theta^*} - \Sigma_{\theta^* \theta} \Sigma_\theta^{-1} \Sigma_{\theta^* \theta}^T) + \Omega, \text{ an } M \times M \text{ matrix.} \end{aligned}$$

175 Likewise, we define  $\Lambda_i$  and  $\lambda^{(i)}$  as the discrepancy counterparts of  $\Gamma_i$  and  $\gamma^{(i)}$  with the  
 176 covariance parameter  $\boldsymbol{\xi}_d$ . Hence,  $\Lambda_i$  and  $\lambda^{(i)}$  are the  $i$ th block discrepancy covariance  
 177 matrix and the  $(n_i - 1) \times 1$  covariance vector between the block outputs and the block  
 178 mean respectively,

$$\begin{aligned} \{\lambda^{(i)}\}_j &= \sum_{k=1}^{n_i} K_d(\mathbf{s}_{ij}, \mathbf{s}_{ik}; \boldsymbol{\xi}_d) / n_i, \quad j = 1, \dots, n_i - 1, \\ \{\Lambda_i\}_{jk} &= K_d(\mathbf{s}_{ij}, \mathbf{s}_{ik}; \boldsymbol{\xi}_d), \quad j = 1, \dots, n_i - 1, \quad k = 1, \dots, n_i - 1. \end{aligned}$$

179 The conditional mean and covariance for observational data in the  $i$ th block are therefore

$$\begin{aligned} \mu_i^{\mathbf{Z}|\bar{\mathbf{Z}}} &= (\mathbf{I}_{n_i-1} \otimes \Sigma_{\theta^* \theta} \Sigma_\theta^{-1}) \mathbf{Y}_{(i)} + (\tau^{(i)} + \lambda^{(i)}) \left\{ \Sigma^{\bar{\mathbf{Z}}} \right\}_{ii}^{-1} (\bar{\mathbf{Z}}_i - \left\{ \mu^{\bar{\mathbf{Z}}} \right\}_i), \\ \Sigma_i^{\mathbf{Z}|\bar{\mathbf{Z}}} &= (\Gamma_i \otimes (\Sigma_{\theta^*} - \Sigma_{\theta^* \theta} \Sigma_\theta^{-1} \Sigma_{\theta^* \theta}^T) + \Lambda_i) - (\tau^{(i)} + \lambda^{(i)}) (\tau^{(i)} + \lambda^{(i)})^T / \left\{ \Sigma^{\bar{\mathbf{Z}}} \right\}_{ii}, \end{aligned}$$

180 where  $\tau^{(i)} = \gamma^{(i)} \otimes (\Sigma_{\theta^*} - \Sigma_{\theta^* \theta} \Sigma_\theta^{-1} \Sigma_{\theta^* \theta}^T)$ . The log composite likelihood for the observa-

181 tional data is then

$$\begin{aligned}
cl_n(\boldsymbol{\psi}) \propto & -\frac{1}{2} \left( \log |\Sigma^{\bar{\mathbf{z}}}| + (\bar{\mathbf{z}} - \mu^{\bar{\mathbf{z}}})^T (\Sigma^{\bar{\mathbf{z}}})^{-1} (\bar{\mathbf{z}} - \mu^{\bar{\mathbf{z}}}) \right) \\
& - \frac{1}{2} \sum_{i=1}^M \left( \log |\Sigma_i^{\mathbf{z}|\bar{\mathbf{z}}}| + (\mathbf{z}_{(i)} - \mu_i^{\mathbf{z}|\bar{\mathbf{z}}})^T (\Sigma_i^{\mathbf{z}|\bar{\mathbf{z}}})^{-1} (\mathbf{z}_{(i)} - \mu_i^{\mathbf{z}|\bar{\mathbf{z}}}) \right),
\end{aligned} \tag{3}$$

182 where the first line in (3) is the log likelihood corresponding to the block means and  
183 the second line corresponding to the observations within each block.  $\boldsymbol{\psi}$  denotes all the  
184 parameters being estimated in the calibration stage including  $\boldsymbol{\theta}^*$  and  $\boldsymbol{\xi}_d$ . By choosing a  
185 proper prior for  $\boldsymbol{\psi}$ ,  $f(\boldsymbol{\psi})$ , we define the approximate log posterior density,  $\log(\pi_n(\boldsymbol{\psi})) \propto$   
186  $\log f(\boldsymbol{\psi}) + cl_n(\boldsymbol{\psi})$  and infer  $\boldsymbol{\psi}$  using the standard Metropolis-Hastings algorithm. We  
187 allow the scale parameters for the emulator to be re-estimated along with the other  
188 parameters but fix the other emulator parameters in  $\boldsymbol{\xi}_s$  at their estimated values from  
189 the emulation stage (Bayarri et al., 2007; Bhat et al., 2012; Chang et al., 2013). The  
190 formulation results in the same computation gain as in the emulation stage.

191 In both the emulation and calibration stages, calculation of the covariance matrix  
192 for the block means is a computational bottleneck, requiring  $\sum_{i=1}^M \sum_{j=i}^M n_i n_j$  flops of  
193 computation. While computationally very demanding, its contribution to the likelihood  
194 function is usually not significant (Caragea and Smith, 2006). Therefore, instead of using  
195 all cross covariances between spatial locations, we randomly sample a subset of cross  
196 covariances to approximate the covariance between block means  $\mathbf{H}$ . The computation of  
197  $\mathbf{H}$  in (2) is substituted by

$$\{\mathbf{H}\}_{ij} = \frac{1}{m_i m_j} \sum_{k=1}^{m_i} \sum_{l=1}^{m_j} K_s(\mathbf{u}_{ik}, \mathbf{u}_{jl}; \boldsymbol{\xi}_s), \tag{4}$$

198 with  $m_i \leq n_i$  and  $m_j \leq n_j$ , where  $\mathbf{u}_{i1}, \dots, \mathbf{u}_{im_i}$  and  $\mathbf{u}_{j1}, \dots, \mathbf{u}_{jm_j}$  are randomly chosen  
199 respectively from  $\mathbf{s}_{i1}, \dots, \mathbf{s}_{in_i}$  and  $\mathbf{s}_{j1}, \dots, \mathbf{s}_{jn_j}$ . This reduces the computational cost from  
200  $\sum_{i=1}^M \sum_{j=i}^M n_i n_j$  to  $\sum_{i=1}^M \sum_{j=i}^M m_i m_j$ , that is,  $1.32 \times 10^7$  flops to  $2.86 \times 10^5$  flops for the  
201 calibration problem in Section 4. The same approximation can be applied to  $\Omega$  with  $\boldsymbol{\xi}_d$ .

**Covariance Function and Prior Specification.** We use the exponential covariance  
function to define the covariance between parameter settings ( $K_\theta$ ), spatial covariance for

the emulator ( $K_s$ ), and the spatial covariance for the discrepancy ( $K_d$ ) with a nugget term. To be more specific, the covariance between the process at two parameter settings  $\boldsymbol{\theta} = (\theta_1, \dots, \theta_q)^T$  and  $\boldsymbol{\theta}' = (\theta'_1, \dots, \theta'_q)^T$  is defined by

$$K_\theta(\boldsymbol{\theta}, \boldsymbol{\theta}'; \boldsymbol{\xi}_\theta) = \zeta_\theta 1(\boldsymbol{\theta} = \boldsymbol{\theta}') + \kappa_\theta \exp\left(-\sum_{i=1}^q \phi_{\theta,i} |\theta_i - \theta'_i|\right),$$

202 where  $\boldsymbol{\xi}_\theta = (\zeta_\theta, \kappa_\theta, \phi_{\theta,1}, \dots, \phi_{\theta,q})$ , and  $\zeta_\theta, \kappa_\theta, \phi_{\theta,1}, \dots, \phi_{\theta,q} > 0$ . Likewise, the covariance  
 203 between the process at two spatial locations  $\mathbf{s}$  and  $\mathbf{s}'$  for the emulator and the discrepancy  
 204 term are given by

$$K_s(\mathbf{s}, \mathbf{s}'; \boldsymbol{\xi}_s) = \kappa_s (\zeta_s 1(\mathbf{s} = \mathbf{s}') + \exp(-\phi_s g(\mathbf{s}, \mathbf{s}'))),$$

205 and

$$K_d(\mathbf{s}, \mathbf{s}'; \boldsymbol{\xi}_d) = \kappa_d (\zeta_d 1(\mathbf{s} = \mathbf{s}') + \exp(-\phi_d g(\mathbf{s}, \mathbf{s}'))), \quad (5)$$

206 respectively, with  $\boldsymbol{\xi}_s = (\zeta_s, \kappa_s, \phi_s)$ ,  $\boldsymbol{\xi}_d = (\zeta_d, \kappa_d, \phi_d)$ , and  $\zeta_s, \kappa_s, \phi_s, \zeta_d, \kappa_d, \phi_d > 0$ .  $g(\mathbf{s}, \mathbf{s}')$   
 207 denotes the distance between two points. In the climate model calibration problem in  
 208 Section 4, for example,  $g$  is the geodesic distance between two points on the earth's  
 209 surface.

210 The parameters inferred by the Bayesian approach in the calibration stage are  $\kappa_s$ ,  
 211  $\zeta_d$ ,  $\kappa_d$ ,  $\phi_d$ , and  $\boldsymbol{\theta}^*$ . Following Bayarri et al. (2007), the sill parameter for the emulator  
 212  $\kappa_s$  is initially inferred via maximum likelihood estimate in the emulation stage and re-  
 213 estimated by Bayesian inference in the calibration stage. We impose informative priors  
 214 on the above parameters to avoid potentially obtaining improper posterior distributions  
 215 (cf. Berger et al., 2001) and identifiability issues. The latter is explained further in  
 216 Section 4. The sill parameters,  $\kappa_s$  and  $\kappa_d$  receive inverse-Gamma priors  $IG(a_{\kappa_s}, b_{\kappa_s})$   
 217 and  $IG(a_{\kappa_d}, b_{\kappa_d})$ . We also impose an Inverse-Gamma prior  $IG(a_{\zeta_d}, b_{\zeta_d})$  for the nugget  
 218 parameter  $\zeta_d$ . The prior density for the range parameter  $\phi_d$  is assumed to be uniform  
 219 with a wide support. The fitted computer model parameter  $\boldsymbol{\theta}^*$  also receives a uniform

220 prior over a wide range. Note that one can also assume a more informative prior for  
 221  $\boldsymbol{\theta}^*$  such as a unimodal distribution based on some physical knowledge. However, in the  
 222 calibration problem in Section 4 we do not impose such a prior for  $\boldsymbol{\theta}^*$ ; this allows us to  
 223 study the characteristics of the posterior density of  $\boldsymbol{\theta}^*$  more transparently.

224 **Asymptotics and Adjustment using Godambe Information.** Note that the com-  
 225 posite likelihood in (3) is not based on the true probability model in (1), and therefore the  
 226 ‘composite’ posterior density based on (3) is quite different from the true posterior based  
 227 on (1). In this section, we will discuss how the Godambe information matrix (Godambe,  
 228 1960) for estimating equations may be used to adjust for using the composite likelihood  
 229 when making inferences.

We first provide the asymptotic justification for the adjustment using the Godambe  
 information matrix. We will show that, for large  $n$  and  $p$ , the mode of the approximate  
 posterior  $\hat{\boldsymbol{\psi}}_n^B = \arg \max_{\boldsymbol{\psi}} \pi_n(\boldsymbol{\psi})$  is consistent and asymptotically normally distributed  
 with a covariance matrix given by the inverse of the Godambe information matrix. If we  
 let  $p \rightarrow \infty$ , then the emulator converges to the measurement-error model such that

$$\boldsymbol{\eta}(\boldsymbol{\theta}) \sim N(\mathbf{Y}(\boldsymbol{\theta}), \zeta_{\theta} \Sigma^s),$$

230 where  $\mathbf{Y}(\boldsymbol{\theta})$  is the  $n \times 1$  vector of model output at the parameter setting  $\boldsymbol{\theta}$  and the  
 231 spatial locations  $\mathbf{s}_1, \dots, \mathbf{s}_n$ . This result holds as long as the computer model output  
 232 varies reasonably smoothly in the parameter space (Yakowitz and Szidarovszky, 1985).  
 233 The model for observational data becomes

$$\mathbf{Z} \sim N(\mathbf{Y}^*, \zeta_{\theta} \Sigma^s + \Sigma^d), \tag{6}$$

234 where  $\mathbf{Y}^* = \mathbf{Y}(\boldsymbol{\theta}^*)$ . The composite likelihood in (3) then has the following means and  
 235 covariances,

$$\begin{aligned} \mu^{\bar{\mathbf{Z}}} &= \bar{\mathbf{Y}}^*, \text{ an } M \times 1 \text{ vector,} \\ \Sigma^{\bar{\mathbf{Z}}} &= \zeta_{\theta} \mathbf{H} + \Omega, \text{ an } M \times M \text{ matrix,} \end{aligned}$$

$$\begin{aligned}\mu_i^{\mathbf{Z}|\bar{\mathbf{Z}}} &= \mathbf{Y}_{(i)}^* + (\zeta_\theta \gamma^{(i)} + \lambda^{(i)}) \left\{ \Sigma^{\bar{\mathbf{Z}}} \right\}_{ii}^{-1} (\bar{\mathbf{Z}}_i - \left\{ \mu^{\bar{\mathbf{Z}}} \right\}_i), \\ \Sigma_i^{\mathbf{Z}|\bar{\mathbf{Z}}} &= (\zeta_\theta \Gamma_i + \Lambda_i) - (\zeta_\theta \gamma^{(i)} + \lambda^{(i)}) (\zeta_\theta \gamma^{(i)} + \lambda^{(i)})^T / \left\{ \Sigma^{\bar{\mathbf{Z}}} \right\}_{ii},\end{aligned}$$

236 where  $\bar{\mathbf{Y}}_{(i)}^* = \frac{1}{n_i} \sum_{j=1}^{n_i} Y(\mathbf{s}_{ij}, \boldsymbol{\theta}^*)$  is the  $i$ th block mean of the computer model output at  
237  $\boldsymbol{\theta}^*$  and  $\bar{\mathbf{Y}}^* = \left( \bar{\mathbf{Y}}_{(1)}^*, \dots, \bar{\mathbf{Y}}_{(M)}^* \right)^T$  is the collection of all their block means.

238 We now show the consistency and the asymptotic normality of the posterior mode  
239  $\hat{\boldsymbol{\psi}}_n^B$  as  $n \rightarrow \infty$ . We utilize expanding domain asymptotic results (see e.g. Mardia and  
240 Marshall, 1984; Cressie, 1993; Cox and Reid, 2004; Zhang and Zimmerman, 2005; Varin,  
241 2008). The first step is establishing consistency and asymptotic normality of the maxi-  
242 mum composite likelihood estimator.

**Proposition 1.** *The following holds for the maximum composite likelihood estimator*

$$\hat{\boldsymbol{\psi}}_n^{CL} = \arg \max_{\boldsymbol{\psi}} cl_n(\boldsymbol{\psi});$$

(i) (Consistency) *The maximum composite likelihood estimator is consistent for  $\boldsymbol{\psi}^0$ ;*

$$\hat{\boldsymbol{\psi}}_n^{CL} \xrightarrow{\mathcal{P}} \boldsymbol{\psi}^0,$$

as  $n \rightarrow \infty$ , where  $\boldsymbol{\psi}^0$  is the vector of true values of parameters in  $\boldsymbol{\psi}$ .

(ii) (Asymptotic Normality) *The asymptotic distribution of the maximum composite likelihood estimator is given by*

$$\mathbf{G}_n^{\frac{1}{2}} \left( \hat{\boldsymbol{\psi}}_n^{CL} - \boldsymbol{\psi}^0 \right) \xrightarrow{\mathcal{D}} N(0, \mathbf{I}),$$

243 where  $\mathbf{G}_n = \mathbf{Q}_n \mathbf{P}_n^{-1} \mathbf{Q}_n$  is the Godambe information matrix (Godambe, 1960).  $\mathbf{P}_n$  is  
244 the covariance matrix of the gradient  $\nabla cl_n$  and  $\mathbf{Q}_n$  is the negative expected value of the  
245 Hessian matrix of  $cl_n$ , where both are evaluated at  $\boldsymbol{\psi} = \boldsymbol{\psi}^0$ .

246 *Proof.* For a composite likelihood, it is sufficient to verify the same regularity conditions as  
247 for the usual maximum likelihood estimators (Lindsay, 1988). In the context of expanding  
248 domain asymptotics in spatial statistics, the spatial covariance function and its first and  
249 second derivatives need to be absolutely summable. From Theorem 3 in Mardia and

250 Marshall (1984), this condition holds for the exponential covariance function that we are  
 251 using here. (i) and (ii) follow immediately.  $\square$

252 We are ready to state the main result of this section, which establishes the consistency  
 253 and asymptotic normality of the posterior mode,  $\hat{\boldsymbol{\psi}}_n^B$ .

254 **Proposition 2.** (i) (Posterior consistency) The posterior degenerates on the true value  
 255  $\boldsymbol{\psi}^0$  in total variation, i.e.

$$|\pi_n(\boldsymbol{\psi}) - \pi_n^0(\boldsymbol{\psi})|_{TV} \xrightarrow{\mathcal{P}} 0 \quad (7)$$

256 as  $n \rightarrow \infty$  where  $|\cdot|_{TV}$  is the total variation norm and  $\pi_n^0(\boldsymbol{\psi})$  is a normal density with  
 257 the mean  $\boldsymbol{\psi}^0 + \mathbf{Q}_n^{-1} \nabla \text{cl}_n(\boldsymbol{\psi}^0)$  and the covariance  $\mathbf{Q}_n^{-1}$ . Note that  $\mathbf{Q}_n^{-1} \rightarrow \mathbf{0}$  as  $n \rightarrow \infty$ .

258 (ii) (Asymptotic normality) The density of  $\hat{\boldsymbol{\psi}}_n^B$  is asymptotically normal;

$$\mathbf{G}_n^{\frac{1}{2}} \left( \hat{\boldsymbol{\psi}}_n^B - \boldsymbol{\psi}^0 \right) \xrightarrow{\mathcal{D}} N(0, \mathbf{I}), \quad (8)$$

259 as  $n \rightarrow \infty$ .

260 *Proof.* When the maximum composite likelihood estimator  $\boldsymbol{\psi}_n^{CL}$  is consistent and asymp-  
 261 totically normal, (i) and (ii) follow (Theorems 1 and 2 respectively in Chernozhukov and  
 262 Hong, 2003). Hence the result follows directly from Proposition 1.  $\square$

263 **Application of Gobambe Adjustment.** We have several options for adjusting our  
 264 composite likelihood-based inference. These include (a) direct use of the asymptotic dis-  
 265 tribution in (8); (b) ‘open-faced sandwich’ post-hoc adjustment (Shaby, 2012) of MCMC  
 266 sample from the composite posterior distribution  $\pi_n(\boldsymbol{\psi})$ ; (c) ‘curvature’ adjustment (Coo-  
 267 ley et al., 2011) for our MCMC procedure. We will utilize (b) and (c) because these  
 268 MCMC-based methods can capture the higher-order moments of the posterior distribu-  
 269 tion, which may be important in finite sample inference.

270 For any of these methods, it is necessary to evaluate  $\mathbf{P}_n$  and  $\mathbf{Q}_n$ . See the appendix  
 271 for an example of their analytic computation. Note that  $\mathbf{Q}_n$  can also be obtained using  
 272 MCMC runs from the posterior distribution  $\pi_n(\boldsymbol{\psi})$  by the asymptotic result in (7).

273 We caution that the adjustment procedures here rely on the identifiability of param-  
 274 eters in  $\boldsymbol{\psi}$ . In order to evaluate  $\mathbf{P}_n$  and  $\mathbf{Q}_n$  under the correct probability model in (6),  
 275 we need to be able to estimate the true value  $\boldsymbol{\psi}^0$  accurately by the posterior mode  $\hat{\boldsymbol{\psi}}_n^B$ .  
 276 This may not always hold as there is a trade-off between the discrepancy parameters in  
 277  $\boldsymbol{\xi}_d$  for finite sample sizes.

278 The open-faced sandwich adjustment is one approach for adjusting the covariance  
 279 based on Proposition 2 (Shaby, 2012). For any MCMC sample of  $\boldsymbol{\psi}$  from  $\pi_n(\boldsymbol{\psi})$ , the open-  
 280 faced sandwich adjustment is defined by  $\tilde{\boldsymbol{\psi}}^{open} = \hat{\boldsymbol{\psi}}_n^B + \mathbf{C}(\boldsymbol{\psi} - \hat{\boldsymbol{\psi}}_n^B)$  with  $\mathbf{C} = \mathbf{Q}_n^{-1}\mathbf{P}_n^{\frac{1}{2}}\mathbf{Q}_n^{\frac{1}{2}}$ .  
 281 Similar to the curvature adjustment, this approach guarantees that the distribution of  
 282 the adjusted posterior sample has the same posterior mode and the desired asymptotic  
 283 covariance  $\mathbf{G}_n^{-1}$ . Note that this method can be either embedded in each step of MCMC  
 284 run or applied after an entire MCMC run is finished.

285 Another approach is curvature adjustment (Cooley et al., 2011), which substitutes  $\boldsymbol{\psi}$   
 286 in (3) with  $\tilde{\boldsymbol{\psi}}^{curv} = \hat{\boldsymbol{\psi}}_n^B + \mathbf{D}(\boldsymbol{\psi} - \hat{\boldsymbol{\psi}}_n^B)$ , where  $\boldsymbol{\psi}$  is the posterior mode from (3).  $\mathbf{D}$  is  
 287 the matrix that satisfies  $\mathbf{D}^T\mathbf{Q}_n\mathbf{D} = \mathbf{Q}_n\mathbf{P}_n^{-1}\mathbf{Q}_n$ . This approach ensures that the resulting  
 288 posterior distribution has the same mode as the original composite likelihood  $c\ell_n(\boldsymbol{\psi})$  and  
 289 the asymptotic covariance  $\mathbf{G}_n^{-1}$  as described in (8). Note that the choice for  $\mathbf{D}$  is not  
 290 unique, and Cooley et al. (2011) suggested using  $\mathbf{D} = \mathbf{Q}_n^{\frac{1}{2}}(\mathbf{Q}_n\mathbf{P}_n^{-1}\mathbf{Q}_n)^{\frac{1}{2}}$  where the square  
 291 roots of the matrices are computed using singular value decomposition. Here we use  
 292 the open-faced adjustment; the curvature adjustment approach may also be used but,  
 293 as shown in (Shaby, 2012), the difference between the two approaches is likely to be  
 294 minimal.

## 295 4 Application to UVic ESCM Calibration

296 We demonstrate the application of our approach to a climate model calibration problem.  
 297 The computer model used here is the University of Victoria Earth system climate model  
 298 (UVic ESCM) of intermediate complexity (Weaver et al., 2001). The input parameter  
 299 that we are interested in is climate sensitivity (CS), defined as the equilibrium global

300 mean surface air temperature change due to a doubling of carbon dioxide concentrations  
301 in the atmosphere (Andronova et al., 2007; Knutti and Hegerl, 2008). Climate sensitivity  
302 is an important model diagnostic and used as an input to climate projections as well  
303 as economic assessments of climate change impacts (see e.g. Nordhaus and Boyer, 2000;  
304 Keller et al., 2004). Each model run is a spatial pattern of ocean temperature anomaly  
305 on a regular  $1.8^\circ$  latitude by  $3.6^\circ$  longitude grid, defined as change between 1955-1964  
306 mean and 2000-2009 mean in degree Celsius times meter ( $^\circ\text{C m}$ ). At each location, the  
307 ocean temperature anomaly is vertically integrated from 0 to 2000 m. in depth.

308 Note that the model output has regions of missing data since it covers only the ocean,  
309 and partition of the spatial area needs careful consideration. We partition the spatial area  
310 using a random tessellation; this is also the approach followed by Eidsvik et al. (2013).  
311 We first randomly choose  $M$  different centroids out of total  $n$  locations and then assign  
312 the spatial locations to different subregions according to the nearest centroid in terms of  
313 geodesic distance. When finding the nearest centroid for each point, we only consider the  
314 centroids in the same ocean to avoid assigning locations separated by land to the same  
315 block. This random tessellation ensures, on average, that we have more subregions where  
316 data points are more densely distributed.

## 317 **4.1 Simulated Examples**

318 We conducted some perfect model experiments to answer the following questions: (i)  
319 Is the posterior density based on the composite likelihood (composite posterior) similar  
320 to the posterior density based on the original likelihood (original posterior)? (ii) Is the  
321 posterior density with approximated block mean covariance computation (approximated  
322 composite posterior) described in (4) close to the true composite posterior? (iii) How do  
323 the number of spatial blocks and the magnitude of the discrepancy affect the composite  
324 posterior density?

325 Each experiment follows four key steps below:

- 326 1. Choose one of the parameter settings for model runs as the synthetic truth.



- 327 2. Leave the corresponding model run out and superimpose a randomly generated  
328 error on it to construct a synthetic observation.
- 329 3. Emulate the computer model using the remaining model runs.
- 330 4. Calibrate the computer model using the emulator in 3 and compare the resulting  
331 density with the synthetic truth.

332 To be able to compute the original posterior density with a reasonable computational  
333 effort, we restrict ourselves to a subset of spatial locations consisting of 1000 randomly  
334 selected points and assume separable covariance structure for the spatial field and the  
335 computer model parameter space. The synthetic truth for the climate sensitivity used  
336 here is 2.153, but choosing other parameter settings gives similar results shown here.

337 A comparison between the composite posterior densities with 10 blocks and the orig-  
338 inal posterior densities are shown in Figure 1(a) and 1(b). We used two different  
339 realizations of the model-observation discrepancy. These were generated from a Gaussian  
340 process model with exponential covariance (5) with  $\zeta_d^* = 0.01$ ,  $\kappa_d^* = 160000$ , and  $\phi_d^* = 690$   
341 km, where  $(\zeta_d^*, \kappa_d^*, \phi_d^*)$  are assumed true values of  $(\zeta_d, \kappa_d, \phi_d)$ . We also conducted the same  
342 comparison for the approximated composite posterior densities (Figure 1(c) and 1(d)).  
343 The posterior densities and the resulting credible intervals from all three approaches are  
344 reasonably similar. The composite posterior densities after adjustment are slightly more  
345 dispersed than the original posterior due to the information loss caused by blocking,  
346 but the modes are quite close to the original ones confirming the consistency result in  
347 Proposition 2 (i).

348 We also compared the adjusted composite posterior densities with different numbers  
349 of blocks to examine the effect of the number of blocks on calibration results (Figure 2).  
350 The results show that using more than 30 blocks introduce a slight bias for the posterior  
351 mode which might be due to the reduced number of data points in each block. However,  
352 the credible intervals are again reasonably similar to each other. Similarly, we compare  
353 the adjusted composite posterior densities based on datasets generated using different  
354 assumed sill values,  $\kappa_d^* = 40000, 90000$  and  $160000$  to investigate the effect of magnitude

355 of discrepancy on calibration results (Figure 3). As one would expect, the posterior  
356 density becomes more dispersed as we increase the value of the sill.

357 We used informative priors for the statistical parameters, which is important to reduce  
358 the identifiability issues occurring in the calibration based on observational data in Section  
359 4.2. We imposed a vague prior for the nugget parameter  $\zeta_d \sim IG(2, 0.01(2 + 1))$  and a  
360 highly informative prior for the sill parameter  $\kappa_d \sim IG(10000, \kappa_d^*(10000 + 1))$ . The sill  
361 parameter for the emulator  $\kappa_s$  is given a mildly informative prior with  $IG(20, \hat{\kappa}_s(20 + 1))$ ,  
362 where  $\hat{\kappa}_s$  is the MLE of  $\kappa_s$  computed in the emulated stage. The shape parameters for the  
363 inverse-Gamma distributions are specified in the way that the prior modes are aligned  
364 with certain target values. Note that inference for simulated examples does not suffer  
365 from identifiability issues without the informative priors; we use these priors only to be  
366 consistent with the calibration based on observational data below.

## 367 4.2 Calibration using Observational Data

368 As an illustrative example, we calibrate the climate sensitivity using the observed spatial  
369 pattern of ocean temperature anomaly from the data product constructed by Levitus  
370 et al. (2012). We interpolated the observational data onto the UVic model grid using  
371 a simple bilinear interpolator. This step allows us to assume separability of emulation  
372 error and spatial covariance. We divide the 5,903 locations into 50 blocks using the ran-  
373 dom tessellation method described above. The covariance matrices for block means are  
374 approximated using (4) with  $m_i = \min(10, n_i)$  for  $i = 1, \dots, 50$ . The prior specification  
375 is the same as the simulated example with assumed sill ( $\kappa_d^*$ ) of 160,000, except that the  
376 discrepancy range parameter  $\phi_d$  is restricted to be greater than 800 km to reduce iden-  
377 tifiability issues. Figure 4 shows the posterior density of climate sensitivity. The length  
378 of the MCMC chain is 15,000, and the computing time is about 15 hours (wall time) via  
379 parallel computing using 32 high-performance cores for a system with Intel Xeon E5450  
380 Quad-Core 434 at 3.0 GHz. We verified that our MCMC algorithm and chain length  
381 were adequate by ensuring that the MCMC standard errors for our parameter estimates  
382 (Jones et al., 2006; Flegal et al., 2008) are small enough and by comparing posterior

383 density estimates after various run lengths to see that the results, namely posterior pdfs,  
384 have stabilized.

## 385 **5 Discussion**

### 386 **5.1 Summary and future direction**

387 This work is, to our knowledge, the first application of composite likelihood to the com-  
388 puter model calibration problem. Our composite likelihood approach enables computa-  
389 tionally efficient inference in computer model calibration using high-dimensional spatial  
390 data. We proved consistency and asymptotic normality of our posterior estimates and  
391 established covariance adjustment for posterior density based on them. The adjustment  
392 can be easily integrated into common MCMC algorithms such as the Metropolis-Hastings  
393 algorithm. The block composite likelihood used here yields a valid probability model, and  
394 therefore no additional verification for the propriety of the posterior distribution is nec-  
395 essary.

396 An attractive benefit of this general framework is that it is relatively easy, in principle,  
397 to extend the approach to a more complicated and easy-to-interpret covariance model.  
398 For example, by allowing covariance parameters to vary across the different spatial blocks,  
399 our approach can introduce non-stationarity in the spatial processes of model output and  
400 observational data.

### 401 **5.2 Caveats**

402 While our approach is helpful in mitigating computational issues for various calibration  
403 problems, there is still more work to be done to make the computation more efficient.  
404 As  $n$  continues to get large the number of spatial locations in each block may become  
405 excessively large and evaluation of composite likelihood may not be computationally  
406 tractable. One may consider increasing the number of blocks until the computation  
407 becomes feasible, but then the convergence of the posterior modes may be very slow due  
408 to too small block sizes (Cox and Reid, 2004; Varin, 2008). Another perhaps simpler

409 approach is to use a composite likelihood framework that does not involve blocks though  
410 this may involve the need for analytical work to establish posterior propriety.

411 Another possible issue is related to the use of a Gaussian emulator in place of the  
412 true computer model in computing  $\mathbf{P}_n$  and  $\mathbf{Q}_n$ . Using a Gaussian process emulator,  
413 we approximate not only the true computer model itself, but also its first and second  
414 derivatives. In our particular example above, this does not cause any problem due to  
415 very regular behavior of the computer model output with respect to the input parameters.  
416 Note, however, that this may not be true in general and therefore  $\mathbf{P}_n$  and  $\mathbf{Q}_n$  calculations  
417 may be inaccurate.

418 It is also worth noting that the asymptotic independence between input parameters  
419 and discrepancy parameters does not usually hold in a finite sample. It is well known  
420 that calibration models usually suffer from identifiability issues (Wynn, 2001). One way  
421 to avoid the issues is imposing discrepancy prior information on the discrepancy term  
422 (Arendt et al., 2012) as we did in Section 4.

423 The scientific result shown in 4.2 requires some caution in its interpretation. First,  
424 besides climate sensitivity, climate system response to changes in radiatively active gases  
425 in the atmosphere also depends on the magnitude of the radiative effects of these gases  
426 (“radiative forcing”), and on the vertical mixing of heat into the deep ocean (Hansen  
427 et al., 1985; Knutti et al., 2002; Schmittner et al., 2009; Urban and Keller, 2010). The  
428 parameters controlling both the forcing, and the vertical mixing, were kept fixed in the  
429 model runs we use. Including these additional uncertainties is expected to make the  
430 posterior density of CS more dispersed. The example serves as a demonstration of com-  
431 putational feasibility of our approach when applied to high-dimensional spatial datasets  
432 rather than providing an improved estimate of CS. Second, the variability of the posterior  
433 density is very sensitive to the prior information for the discrepancy term. Note, however,  
434 that this is a common problem for many calibration problems as discussed earlier.

435 **Appendix: Computation of  $\mathbf{P}_n$  and  $\mathbf{Q}_n$ .**

In this supplementary material, we describe the matrix computation for  $\mathbf{P}_n = \text{Cov} \left( c\dot{\ell}_n(\boldsymbol{\psi}) \right)$  and  $\mathbf{Q}_n = \text{E} \left( c\ddot{\ell}_n(\boldsymbol{\psi}) \right)$ . For ease of computation, it is useful to rewrite the composite likelihood function when  $p = \infty$  in the following way:

$$c\ell_n(\boldsymbol{\psi}) \propto -\frac{1}{2} \left( \log |\Sigma^{\bar{\mathbf{Z}}}| + (\bar{\mathbf{Z}} - \bar{\mathbf{Y}}^*)^T \left( \Sigma^{\bar{\mathbf{Z}}} \right)^{-1} (\bar{\mathbf{Z}} - \bar{\mathbf{Y}}^*) \right) - \frac{1}{2} \left( \sum_{i=1}^M \log |\Sigma_i^{\mathbf{Z}|\bar{\mathbf{Z}}}| + \sum_{i=1}^M (\mathbf{Z}_{[i]} - \mathbf{Y}_{[i]}^*)^T \mathbf{A}_i^T \left( \Sigma_i^{\mathbf{Z}|\bar{\mathbf{Z}}} \right)^{-1} \mathbf{A}_i (\mathbf{Z}_{[i]} - \mathbf{Y}_{[i]}^*) \right),$$

where  $\mathbf{A}_i$  is a  $(n_i - 1) \times n_i$  matrix such that

$$\mathbf{A}_i = \left( \mathbf{I}_{(n_i-1) \times (n_i-1)} \mathbf{0}_{(n_i-1) \times 1} \right) - \mathbf{a}_i \left( \frac{1}{n_i}, \dots, \frac{1}{n_i} \right)_{1 \times n_i},$$

and  $\mathbf{a}_i$  is a  $(n_i - 1) \times 1$  vector such that

$$\mathbf{a}_i = \left( \zeta_\theta \gamma^{(i)} + \lambda^{(i)} \right) \left\{ \Sigma^{\bar{\mathbf{Z}}} \right\}_{ii}^{-1}.$$

$\mathbf{Z}_{[i]}$  is a  $n_i \times 1$  vector containing all the  $n_i$  observational data in the  $i$ th spatial block without omission, and  $\mathbf{Y}_{[i]}$  is a  $n_i \times 1$  vector of model output at  $\boldsymbol{\theta}^*$  defined in the same way. Omitting the part irrelevant to the data, the partial derivative of  $c\ell_n(\boldsymbol{\psi})$  with respect to the  $j$ th computer model parameter,  $\theta_j^*$ , is given by

$$\frac{\partial c\ell_n(\boldsymbol{\psi})}{\partial \theta_j^*} \propto \bar{\mathbf{B}}_j^* (\bar{\mathbf{Z}} - \bar{\mathbf{Y}}^*) + \sum_{i=1}^M \mathbf{B}_{i,j}^* (\mathbf{Z}_{[i]} - \mathbf{Y}_{[i]}^*),$$

436 where

$$\begin{aligned} \bar{\mathbf{B}}_j^* &= \frac{\partial \bar{\mathbf{Y}}^*}{\partial \theta_j^*} \left( \Sigma^{\bar{\mathbf{Z}}} \right)^{-1}, \\ \mathbf{B}_{i,j}^* &= \left( \frac{\partial \mathbf{Y}_{[i]}^*}{\partial \theta_j^*} \right)^T \mathbf{A}_i^T \left( \Sigma_i^{\mathbf{Z}|\bar{\mathbf{Z}}} \right)^{-1} \mathbf{A}_i. \end{aligned}$$

437 We let  $\boldsymbol{\xi}$  be the vector containing all the parameters in  $\boldsymbol{\xi}_d$  as well as the emulator pa-  
 438 rameter being re-estimated. The partial derivative with respect to the  $k$ th parameter in  
 439  $\boldsymbol{\xi}$ ,  $\xi_k$ , can be written as

$$\begin{aligned} \frac{\partial cl_n(\boldsymbol{\psi})}{\partial \xi_k} \propto & \frac{1}{2}(\bar{\mathbf{Z}} - \bar{\mathbf{Y}}^*)^T \bar{\mathbf{B}}_k^d (\bar{\mathbf{Z}} - \bar{\mathbf{Y}}^*) \\ & + \frac{1}{2} \sum_{i=1}^M (\mathbf{Z}_{[i]} - \mathbf{Y}_{[i]}^*)^T \mathbf{B}_{i,k}^d (\mathbf{Z}_{[i]} - \mathbf{Y}_{[i]}^*) \\ & + \sum_{i=1}^M (\mathbf{Z}_{[i]} - \mathbf{Y}_{[i]}^*)^T \tilde{\mathbf{B}}_{i,k}^d (\mathbf{Z}_{[i]} - \mathbf{Y}_{[i]}^*) \end{aligned}$$

440 where

$$\begin{aligned} \bar{\mathbf{B}}_k^d &= \left( \Sigma^{\bar{\mathbf{Z}}} \right)^{-1} \frac{\partial \Sigma^{\bar{\mathbf{Z}}}}{\partial \xi_k} \left( \Sigma^{\bar{\mathbf{Z}}} \right)^{-1}, \\ \mathbf{B}_{i,k}^d &= \mathbf{A}_i^T \left( \Sigma_i^{\mathbf{Z}|\bar{\mathbf{Z}}} \right)^{-1} \frac{\partial \Sigma_i^{\mathbf{Z}|\bar{\mathbf{Z}}}}{\partial \xi_k} \left( \Sigma_i^{\mathbf{Z}|\bar{\mathbf{Z}}} \right)^{-1} \mathbf{A}_i, \\ \tilde{\mathbf{B}}_{i,k}^d &= - \left( \frac{\partial \mathbf{A}_i}{\partial \xi_k} \right)^T \left( \Sigma_i^{\mathbf{Z}|\bar{\mathbf{Z}}} \right)^{-1} \mathbf{A}_i. \end{aligned}$$

441 Note that inference on  $\boldsymbol{\theta}^*$ , our main goal, requires only calculating the asymptotic  
 442 covariance of  $\hat{\boldsymbol{\theta}}_n^B$  due to the asymptotic independence between  $\hat{\boldsymbol{\theta}}_n^B$  and  $\hat{\boldsymbol{\xi}}_n^B$ , the posterior  
 443 modes of  $\boldsymbol{\theta}^*$  and  $\boldsymbol{\xi}$  respectively. More specifically, for any  $j$  and  $k$ ,

$$\text{Cov} \left( \frac{\partial cl_n(\boldsymbol{\psi})}{\partial \theta_j^*}, \frac{\partial cl_n(\boldsymbol{\psi})}{\partial \xi_k} \right) = 0,$$

444 because a linear combinations of zero-mean normal random variables and a quadratic  
 445 form of the same variables are uncorrelated to one another. As a result,  $\hat{\boldsymbol{\theta}}_n^B$  and  $\hat{\boldsymbol{\xi}}_n^B$  have  
 446 zero cross-covariance in  $\mathbf{G}_n$  and are asymptotically independent due to normality. Let  $\mathbf{P}_n^*$   
 447 be a part of  $\mathbf{P}_n$ , which is the covariance matrix between partial derivatives with respect  
 448 to the parameters in  $\boldsymbol{\theta}^*$  only. Likewise, let  $\mathbf{Q}_n^*$  be a part of  $\mathbf{Q}_n$  that contains only the  
 449 negative expected Hessian of the parameters in  $\boldsymbol{\theta}^*$ . For inference on  $\boldsymbol{\theta}^*$ , it is sufficient to  
 450 compute  $\mathbf{P}_n^*$  and  $\mathbf{Q}_n^*$  instead of  $\mathbf{P}_n$  and  $\mathbf{Q}_n$ .

451 We compute the  $(k, l)$ th element of  $\mathbf{P}_n^*$  by plugging in  $\hat{\boldsymbol{\psi}}_n^B$  in place of  $\boldsymbol{\psi}$  in the following

452 expression:

$$\begin{aligned}
\text{Cov} \left( \frac{\partial cl_n(\boldsymbol{\psi})}{\partial \theta_k^*}, \frac{\partial cl_n(\boldsymbol{\psi})}{\partial \theta_l^*} \right) = & \quad \bar{\mathbf{B}}_k^* \Sigma^{\bar{\mathbf{Z}}} (\bar{\mathbf{B}}_l^*)^T \\
& + \sum_{i=1}^M \sum_{j=1}^M \mathbf{B}_{i,k}^* \Sigma_{i,j}^{\mathbf{Z}} (\mathbf{B}_{j,l}^*)^T \\
& + \sum_{i=1}^M \bar{\mathbf{B}}_k^* \Sigma_i^{\bar{\mathbf{Z}}, \mathbf{Z}} (\mathbf{B}_{i,l}^*)^T \\
& + \sum_{i=1}^M \bar{\mathbf{B}}_l^* \Sigma_i^{\bar{\mathbf{Z}}, \mathbf{Z}} (\mathbf{B}_{i,k}^*)^T,
\end{aligned}$$

453 where  $\Sigma_{i,j}^{\mathbf{Z}}$  is the  $n_i \times n_j$  covariance matrix between  $\mathbf{Z}_{[i]}$  and  $\mathbf{Z}_{[j]}$ , and  $\Sigma_i^{\bar{\mathbf{Z}}, \mathbf{Z}}$  is the  $1 \times n_i$   
454 covariance matrix between  $\bar{\mathbf{Z}}$  and  $\mathbf{Z}_{[i]}$  under the probability model in (3). Similarly, the  
455 second order partial derivative of  $cl_n(\boldsymbol{\psi})$  with respect to  $\theta_j^*$  and  $\theta_k^*$  is given by

$$\begin{aligned}
\frac{\partial cl_n(\boldsymbol{\psi})}{\partial \theta_j^* \partial \theta_k^*} \propto & \quad \left( \frac{\partial^2 \bar{\mathbf{Y}}^*}{\partial \theta_j^* \partial \theta_k^*} \right)^T (\Sigma^{\bar{\mathbf{Z}}})^{-1} (\bar{\mathbf{Z}} - \bar{\mathbf{Y}}^*) \\
& - \left( \frac{\partial \bar{\mathbf{Y}}^*}{\partial \theta_j^*} \right)^T (\Sigma^{\bar{\mathbf{Z}}})^{-1} \frac{\partial \bar{\mathbf{Y}}^*}{\partial \theta_k^*} \\
& + \sum_{i=1}^M \left( \frac{\partial^2 \mathbf{Y}_{[i]}^*}{\partial \theta_j^* \partial \theta_k^*} \right)^T \mathbf{B}_i^T (\Sigma_i^{\mathbf{Z}|\bar{\mathbf{Z}}})^{-1} \mathbf{B}_i (\mathbf{Z}_{[i]} - \mathbf{Y}_{[i]}^*) \\
& - \sum_{i=1}^M \left( \frac{\partial \mathbf{Y}_{[i]}^*}{\partial \theta_j^*} \right)^T \mathbf{B}_i^T (\Sigma_i^{\mathbf{Z}|\bar{\mathbf{Z}}})^{-1} \mathbf{B}_i \frac{\partial \mathbf{Y}_{[i]}^*}{\partial \theta_k^*}.
\end{aligned}$$

456 The  $(j, k)$ th element of  $\mathbf{Q}_n^*$  is computed by substituting  $\boldsymbol{\psi}$  with  $\hat{\boldsymbol{\psi}}_n^B$  in the following  
457 equation:

$$\begin{aligned}
-E \left( \frac{\partial cl_n(\boldsymbol{\psi})}{\partial \theta_j^* \partial \theta_k^*} \right) \propto & \quad \left( \frac{\partial \bar{\mathbf{Y}}^*}{\partial \theta_j^*} \right)^T (\Sigma^{\bar{\mathbf{Z}}})^{-1} \frac{\partial \bar{\mathbf{Y}}^*}{\partial \theta_k^*} \\
& + \sum_{i=1}^M \left( \frac{\partial \mathbf{Y}_{[i]}^*}{\partial \theta_j^*} \right)^T \mathbf{B}_i^T (\Sigma_i^{\mathbf{Z}|\bar{\mathbf{Z}}})^{-1} \mathbf{B}_i \frac{\partial \mathbf{Y}_{[i]}^*}{\partial \theta_k^*}.
\end{aligned}$$

458 Computing  $\mathbf{P}_n^*$  and  $\mathbf{Q}_n^*$  requires finding the first-order derivatives of  $\mathbf{Y}_{[1]}^*, \dots, \mathbf{Y}_{[M]}^*$ ,  
459 and  $\bar{\mathbf{Y}}^*$ . Since they are unknown functions of  $\boldsymbol{\theta}^*$ , we approximate them using the cor-  
460 responding derivatives of the emulator output. The approximated derivatives of  $\bar{\mathbf{Y}}^*$  and

461  $\mathbf{Y}_{[i]}^*$  with respect to  $\theta_j^*$  are given by

$$\begin{aligned}\frac{\partial \bar{\mathbf{Y}}^*}{\partial \theta_j^*} &= \left( I_M \otimes \left( \frac{\partial \Sigma_{\theta^* \theta}}{\partial \theta_j^*} \Sigma_{\theta}^{-1} \right) \right) \bar{\mathbf{Y}}, \\ \frac{\partial \mathbf{Y}_{[i]}^*}{\partial \theta_j^*} &= \left( I_{n_i} \otimes \left( \frac{\partial \Sigma_{\theta^* \theta}}{\partial \theta_j^*} \Sigma_{\theta}^{-1} \right) \right) \mathbf{Y}_{[i]}.\end{aligned}$$

The derivative term  $\frac{\partial \Sigma_{\theta^* \theta}}{\partial \theta_j^*}$  is determined by the covariance function for the parameter space. For the exponential covariance function used in our example, the derivative is

$$\left\{ \frac{\partial \Sigma_{\theta^* \theta}}{\partial \theta_i^*} \right\}_j = \phi_{\theta, i} (-1)^{1(\theta_i^* > \theta_{ij})} \exp \left( - \sum_{k=1}^q \phi_{\theta, k} |\theta_k^* - \theta_{kj}| \right), \quad i = 1, \dots, q, \quad j = 1, \dots, p,$$

462 where  $1(\cdot)$  is the indicator function, and  $\theta_{ij}$  is the  $i$ th parameter value of the  $j$ th design  
463 point  $\boldsymbol{\theta}_j$ .

464 **Acknowledgment** This work was partly supported by NSF through the Network  
465 for Sustainable Climate Risk Management (SCRiM) under NSF cooperative agreement  
466 GEO-1240507 and the Penn State Center for Climate Risk Management (CLIMA). All  
467 views, errors, and opinions are solely that of the authors.



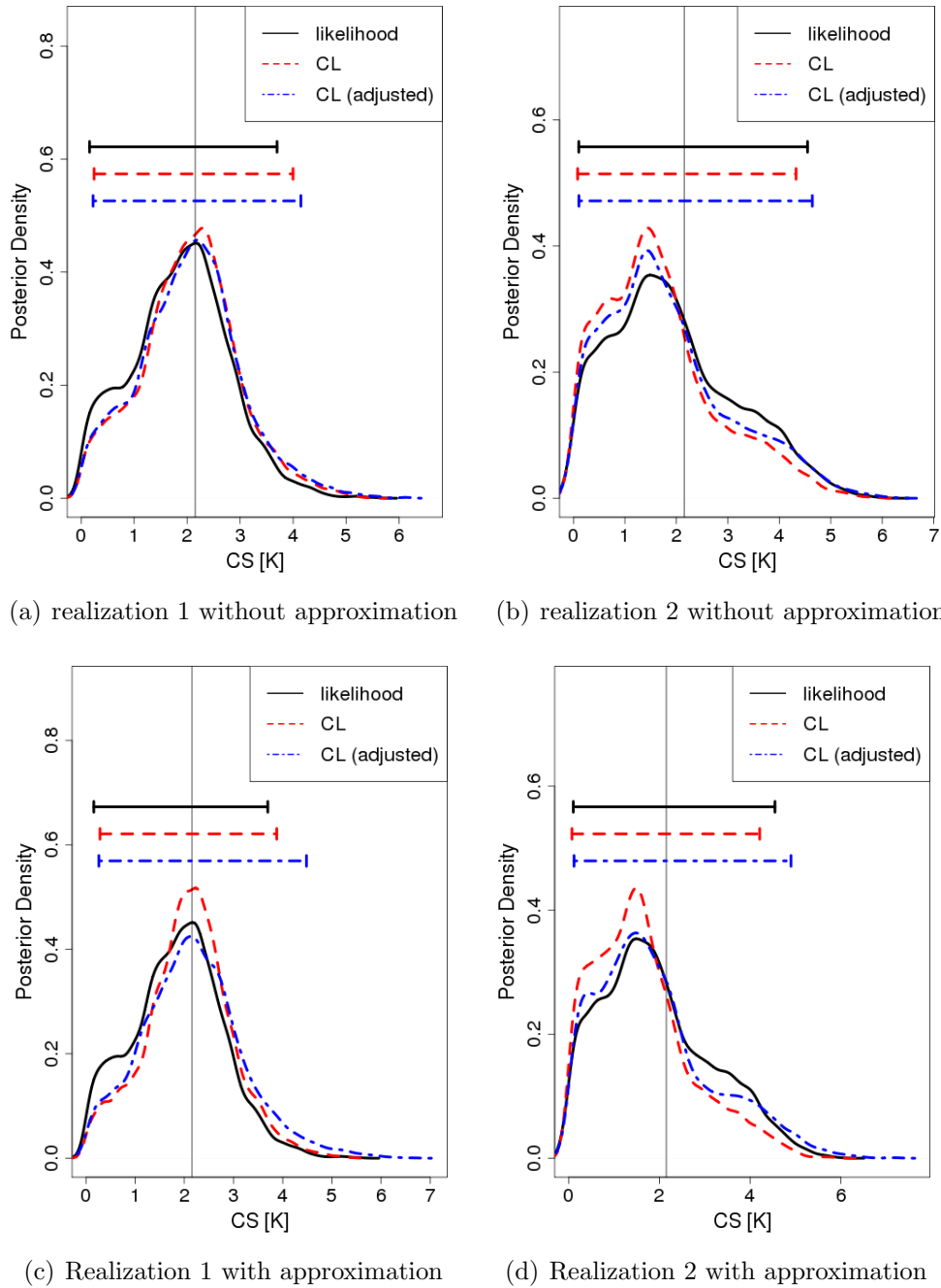


Figure 1: Comparison between calibration results using i) the original likelihood without blocking (solid black curves), ii) the block composite likelihood without the variance adjustment (dashed red line), and iii) the block composite likelihood with the variance adjustment (dashed-dotted blue line). The vertical lines represent the assumed true value for our simulation, and the horizontal bars above show the 95% credible intervals. The results shown here are based on two different realizations (two left panels for Realization 1 and two right panels for Realization 2) from the same GP model. The posterior densities with the approximation for the block means (two lower panels) are reasonably close to the densities without the approximation (two upper panels) when the variance adjustment is applied.

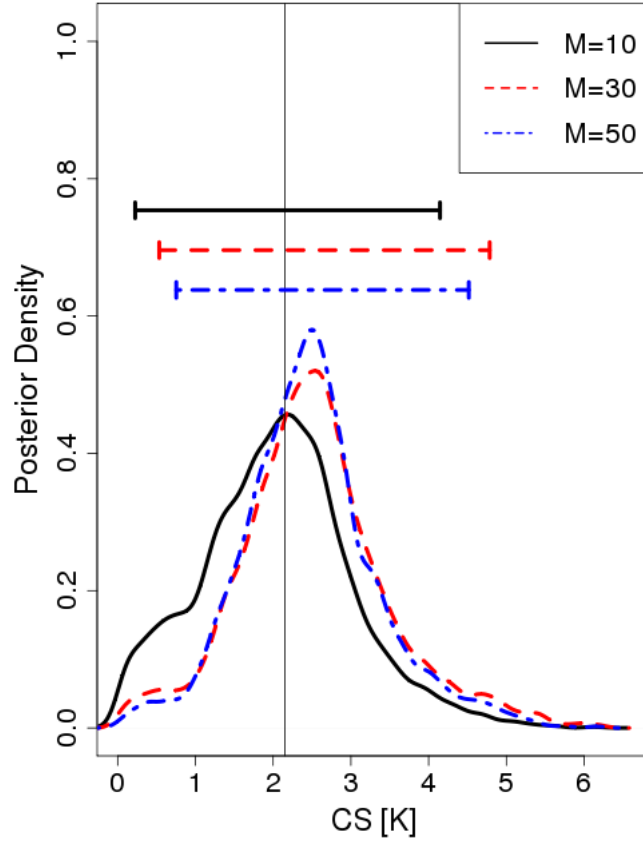


Figure 2: Comparison of posterior densities between three simulated examples with different block numbers:  $M = 10$  (solid black curve),  $M = 30$  (dashed red curve), and  $M = 50$  (dotted-dashed blue curve). The vertical line is the assumed true value for our simulated example and the horizontal bars above are 95% credible intervals. Posterior modes based on 30 and 50 blocks show slight biases, but the width of interval does not show notable differences.

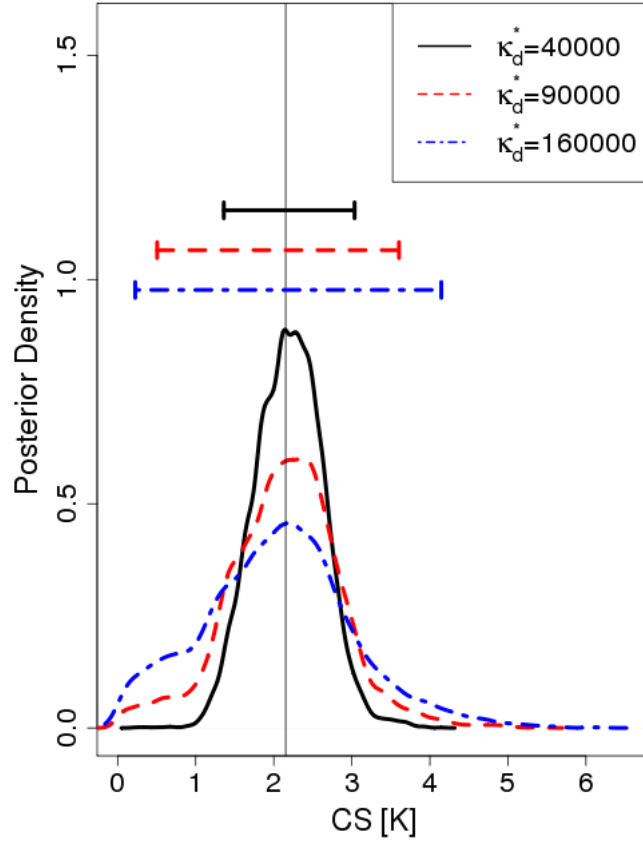


Figure 3: Comparison of posterior densities between three simulated examples with different assumed magnitudes of the discrepancies:  $\kappa_d^* = 40000$  (solid black curve),  $\kappa_d^* = 90000$  (dashed red curve), and  $\kappa_d^* = 160000$  (dotted-dashed blue curve). The vertical line indicates the assumed true values, and the horizontal bars above show the 95% credible intervals. As the discrepancy grows, the densities become more dispersed but the posterior modes stay similar.

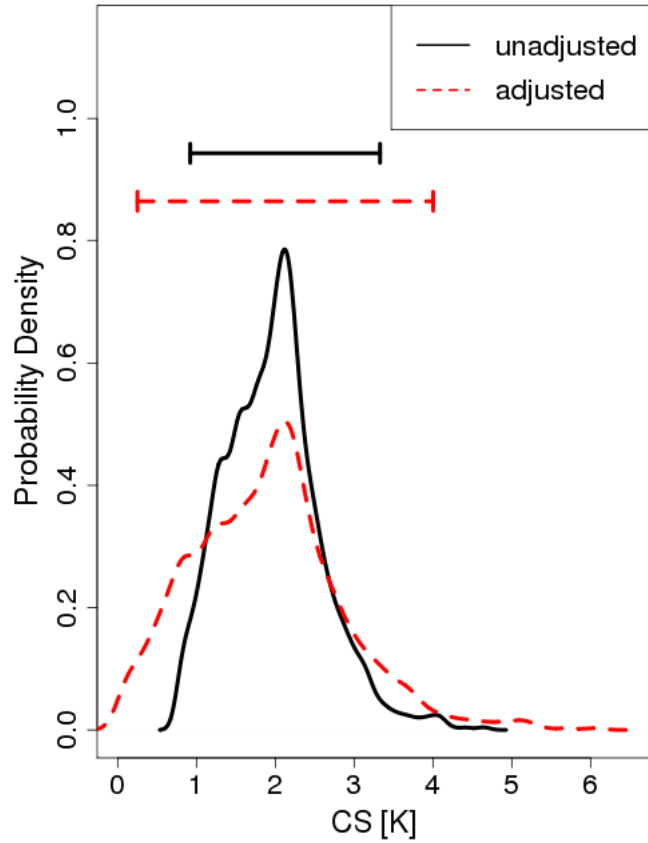


Figure 4: Posterior densities of the climate sensitivity calibrated based on the observational data from Levitus et al. (2012) using our composite likelihood approach. The adjusted posterior density (solid black curve) is notably more dispersed than the unadjusted one (dashed black curve), and the corresponding 95% credible intervals (horizontal bars above) for the adjusted posterior density is also much wider than the one for the unadjusted density.

## 468 References

- 469 Andronova, N., Schlesinger, M., Dessai, S., Hulme, M., and Li, B. (2007), *The concept of*  
470 *climate sensitivity: History and development*, in *Human-induced Climate Change: An*  
471 *Interdisciplinary Assessment*, edited by M. Schlesinger, H. Kheshgi, J. Smith, F. de la  
472 *Chesnaye, J. M. Reilly, T. Wilson, and C. Kolstad*, Cambridge University Press, New  
473 *York*.
- 474 Arendt, P. D., Apley, D. W., and Chen, W. (2012), “Quantification of Model Uncertainty:  
475 Calibration, Model Discrepancy, and Identifiability,” *J. Mech. Design*, 134, 100908.
- 476 Bayarri, M., Berger, J., Cafeo, J., Garcia-Donato, G., Liu, F., Palomo, J., Parthasarathy,  
477 R., Paulo, R., Sacks, J., and Walsh, D. (2007), “Computer model validation with  
478 functional output,” *Ann. Statist.*, 35, 1874–1906.
- 479 Berger, J., De Oliveira, V., and Sansó, B. (2001), “Objective Bayesian analysis of spatially  
480 correlated data,” *J. Am. Statist. Assoc.*, 96, 1361–1374.
- 481 Besag, J. (1975), “Statistical analysis of non-lattice data,” *Statistician*, 24, 179–195.
- 482 — (1977), “Efficiency of pseudolikelihood estimation for simple Gaussian fields,”  
483 *Biometrika*, 64, 616–618.
- 484 Bhat, K., Haran, M., and Goes, M. (2010), “Computer Model Calibration with Multi-  
485 variate Spatial Output: A Case Study,” *Frontiers of Statistical Decision Making and*  
486 *Bayesian Analysis*, 168–184.
- 487 Bhat, K., Haran, M., Olson, R., and Keller, K. (2012), “Inferring likelihoods and climate  
488 system characteristics from climate models and multiple tracers,” *Environmetrics*, 23,  
489 345–362.
- 490 Caragea, P. and Smith, R. (2006), “Approximate likelihoods for spatial processes,”  
491 *Preprint*.
- 492 Chang, W., Haran, M., Olson, R., and Keller, K. (2013), “Fast dimension-reduced climate  
493 model calibration,” *arXiv preprint arXiv:1303.1382*.

494 Chernozhukov, V. and Hong, H. (2003), “An MCMC approach to classical estimation,”  
495 *J. Econometrics*, 115, 293–346.

496 Cooley, D., Ribatet, M., and Davison, A. (2011), “Bayesian inference from composite  
497 likelihoods, with an application to spatial extremes,” *arXiv preprint arXiv:0911.5357*.

498 Cox, D. and Reid, N. (2004), “A note on pseudolikelihood constructed from marginal  
499 densities,” *Biometrika*, 91, 729–737.

500 Cressie, N. (1993), *Statistics for spatial data*, Wiley, New York.

501 Curriero, F. C. and Lele, S. (1999), “A composite likelihood approach to semivariogram  
502 estimation,” *J. Agric. Biol. Environ. Stat.*, 4, 9–28.

503 Eidsvik, J., Shaby, B., Reich, B., Wheeler, M., and Niemi, J. (2013), “Estimation and  
504 prediction in spatial models with block composite likelihoods,” *J. Comp. Graph. Stat.*,  
505 in press.

506 Flegal, J. M., Haran, M., and Jones, G. L. (2008), “Markov chain Monte Carlo: Can we  
507 trust the third significant figure?” *Stat. Sci.*, 23, 250–260.

508 Godambe, V. (1960), “An optimum property of regular maximum likelihood estimation,”  
509 *Ann. Math. Stat.*, 31, 1208–1211.

510 Hansen, J., Russell, G., Lacis, A., Fung, I., Rind, D., and Stone, P. (1985), “Climate  
511 response times - dependence on climate sensitivity and ocean mixing,” *Science*, 229,  
512 857–859.

513 Heagerty, P. J. and Lele, S. R. (1998), “A composite likelihood approach to binary spatial  
514 data,” *J. Am. Statist. Assoc.*, 93, 1099–1111.

515 Higdon, D., Gattiker, J., Williams, B., and Rightley, M. (2008), “Computer model cali-  
516 bration using high-dimensional output,” *J. Am. Statist. Assoc.*, 103, 570–583.

517 Higdon, D., Reese, C., Moulton, J., Vrugt, J., and Fox, C. (2009), “Posterior exploration  
518 for computationally intensive forward models,” *Handbook of Markov Chain Monte*  
519 *Carlo*.

- 520 Jones, G., Haran, M., Caffo, B. S., and Neath, R. (2006), “Fixed-width output analysis  
521 for Markov chain Monte Carlo,” *J. Am. Statist. Assoc.*, 101, 1537–1547.
- 522 Keller, K., Bolker, B., and Bradford, D. F. (2004), “Uncertain climate thresholds and  
523 optimal economic growth,” *J. Environ. Econ. Manage.*, 48, 723–741.
- 524 Kennedy, M. and O’Hagan, A. (2001), “Bayesian calibration of computer models,” *J. R.*  
525 *Stat. Soc. Ser. B Stat. Methodol.*, 63, 425–464.
- 526 Knutti, R. and Hegerl, G. C. (2008), “The equilibrium sensitivity of the Earth’s temper-  
527 ature to radiation changes,” *Nat. Geosci.*, 1, 735–743.
- 528 Knutti, R., Stocker, T. F., Joos, F., and Plattner, G. K. (2002), “Constraints on radiative  
529 forcing and future climate change from observations and climate model ensembles,”  
530 *Nature*, 416, 719–723.
- 531 Levitus, S., Antonov, J., Boyer, T., Baranova, O., Garcia, H., Locarnini, R., Mishonov,  
532 A., Reagan, J., Seidov, D., Yarosh, E., et al. (2012), “World ocean heat content and  
533 thermosteric sea level change (0–2000 m), 1955–2010,” *Geophys. Res. Lett.*, 39.
- 534 Lindsay, B. G. (1988), “Composite likelihood methods,” *Contemp. Math.*, 80, 221–39.
- 535 Mardia, K. V. and Marshall, R. (1984), “Maximum likelihood estimation of models for  
536 residual covariance in spatial regression,” *Biometrika*, 71, 135–146.
- 537 Nordhaus, W. D. and Boyer, J. (2000), *Warning the World: Economic Models of Global*  
538 *Warming*, MIT Press (MA).
- 539 Sacks, J., Welch, W., Mitchell, T., and Wynn, H. (1989), “Design and analysis of com-  
540 puter experiments,” *Stat. Sci.*, 4, 409–423.
- 541 Schmittner, A., Urban, N., Keller, K., and Matthews, D. (2009), “Using tracer observa-  
542 tions to reduce the uncertainty of ocean diapycnal mixing and climate–carbon cycle  
543 projections,” *Global Biogeochem. Cy.*, 23, 737–750.

- 544 Shaby, B. A. (2012), “The open-faced sandwich adjustment for MCMC using estimating  
545 functions,” *arXiv preprint arXiv:1204.3687*.
- 546 Stein, M. L., Chi, Z., and Welty, L. J. (2004), “Approximating likelihoods for large spatial  
547 data sets,” *J. R. Stat. Soc. Ser. B Stat. Methodol.*, 66, 275–296.
- 548 Urban, N. and Keller, K. (2010), “Probabilistic hindcasts and projections of the cou-  
549 pled climate, carbon cycle and Atlantic meridional overturning circulation system: a  
550 Bayesian fusion of century-scale observations with a simple model,” *Tellus A*, 62, 737–  
551 750.
- 552 Varin, C. (2008), “On composite marginal likelihoods,” *Adv. Stat. Anal.*, 92, 1–28.
- 553 Vecchia, A. V. (1988), “Estimation and model identification for continuous spatial pro-  
554 cesses,” *J. R. Stat. Soc. Ser. B Stat. Methodol.*, 50, 297–312.
- 555 Weaver, A., Eby, M., Wiebe, E., Bitz, C., Duffy, P., Ewen, T., Fanning, A., Holland, M.,  
556 MacFadyen, A., and Matthews, H. (2001), “The UVic Earth System Climate Model:  
557 Model description, climatology, and applications to past, present and future climates,”  
558 *Atmos.-Ocean.*, 39, 361–428.
- 559 Wynn, H. (2001), “Contribution to the discussion on the paper by Kennedy and  
560 O’Hagan,” *J. R. Stat. Soc. Ser. B Stat. Methodol.*, 63, 425–464.
- 561 Yakowitz, S. and Szidarovszky, F. (1985), “A comparison of kriging with nonparametric  
562 regression methods,” *J. Multivariate Anal.*, 16, 21–53.
- 563 Zhang, H. and Zimmerman, D. L. (2005), “Towards reconciling two asymptotic frame-  
564 works in spatial statistics,” *Biometrika*, 92, 921–936.